Supporting Information

Meng et al. 10.1073/pnas.1005101107

SI Materials and Methods

Immunostaining for PER2 in Cells. Primary lung fibroblasts were prepared from WT or PER2::Luc transgenic mice as described previously (1). WT lung fibroblasts grown on coverslips were synchronized by 100 nM Dex for 1 h. Cells were then changed to normal culture medium with DMSO or CK1 inhibitor compounds. To decide the peak and trough time of the endogenous PER2 oscillation, parallel dishes of cells went through the same Dex synchronization and were then changed to recording medium for PMT photon counting. Eight hours (peak) or 19 h (trough) later, cells were fixed for indirect immunofluorescence as described previously (1). To evaluate nuclear accumulation and clearance of PER2, semiquantification of fluorescence intensity in grayscale was measured using McMaster Biophotonics Facility Image J software. Results were expressed as relative nuclear intensity ± SEM. Overall, approximately 30 individual cells from three independent experiments were counted.

CK1ε^{tau} Homology Modeling. A CK1ε^{tau} homology model was constructed by superimposing the structure of human CK1δ (1CKI.pdb) (2) onto the *Schizosaccharomyces pombe* CK1-ATP–bound structure (1CSN.pdb) (3) using the secondary-structure alignment tool (4) in the program *Coot* (5). The procedure was then repeated with the PKA–peptide inhibitor cocomplex structure (2CPK.pdb) (6) and compared against the CDK2–peptide substrate structure (1QMZ.pdb) (7) to ensure proper positioning of the peptide group in the catalytic cleft. The seven residues in the catalytic kinase domain that differ between CK1ε and CK1δ were then mutated to reflect the ε sequence and the side chain conformations were minimized using Coot. The same procedure was followed for the τ R178C mutant. The molecular surface of the resulting ATP-bound, CK1ε homology model was then created using an internal structural visualization program, MoViT. (Pfizer) Docking studies of the energy minimized structures of PF-670462 and PF-4800567 in the ATP-binding pocket of the CK1ε homology model were conducted using the MoViT software.

CK1ε and CK1ε^{tau} in Vitro Kinase Assay. The CK1ε and CK1ε^{tau} kinase assays were performed in a 40-μL final volume in buffer containing 50 mM Tris, pH 7.5, 10 mM $MgCl_2$, 1 mM DTT, 100 μg/mL BSA with 10 μM ATP, 2.5 nM CK1ε WT (or 50 nM CK1ε^{tau}), and 42 μM peptide substrate PLSRTLpSVASLPGL (8) in the presence of 1 μL of either inhibitor or 4% dimethyl sulfoxide (negative control). The reaction was incubated for 90 min at 27 °C; detection was carried out as described for the Kinase-Glo Assay (Promega). Luminescent output was measured on the Perkin-Elmer Envision plate reader (PerkinElmer). The results from three independent experiments were conducted and used for statistical analysis.

1. Meng QJ, et al. (2008) Ligand modulation of REV-ERBalpha function resets the peripheral circadian clock in a phasic manner. *J Cell Sci* 121:3629–3635.
2. Longenecker KL, Roach PJ, Hurley TD (1996) Three-dimensional structure of mammalian casein kinase I: Molecular basis for phosphate recognition. *J Mol Biol* 257:618–631.
3. Xu RM, Carmel G, Sweet RM, Kuret J, Cheng X (1995) Crystal structure of casein kinase-1, a phosphate-directed protein kinase. *EMBO J* 14:1015–1023.
4. Krissinel E, Henrick K (2004) Secondary-structure matching (SSM), a new tool for fast protein structure alignment in three dimensions. *Acta Crystallogr D Biol Crystallogr* 60:2256–2268.
5. Emsley P, Cowtan K (2004) Coot: Model-building tools for molecular graphics. *Acta Crystallogr D Biol Crystallogr* 60:2126–2132.
6. Knighton DR, et al. (1991) Structure of a peptide inhibitor bound to the catalytic subunit of cyclic adenosine monophosphate-dependent protein kinase. *Science* 253:414–420.
7. Brown NR, et al. (1999) Effects of phosphorylation of threonine 160 on cyclin-dependent kinase 2 structure and activity. *J Biol Chem* 274:8746–8756.
8. Flotow H, et al. (1990) Phosphate groups as substrate determinants for casein kinase I action. *J Biol Chem* 265:14264–14269.

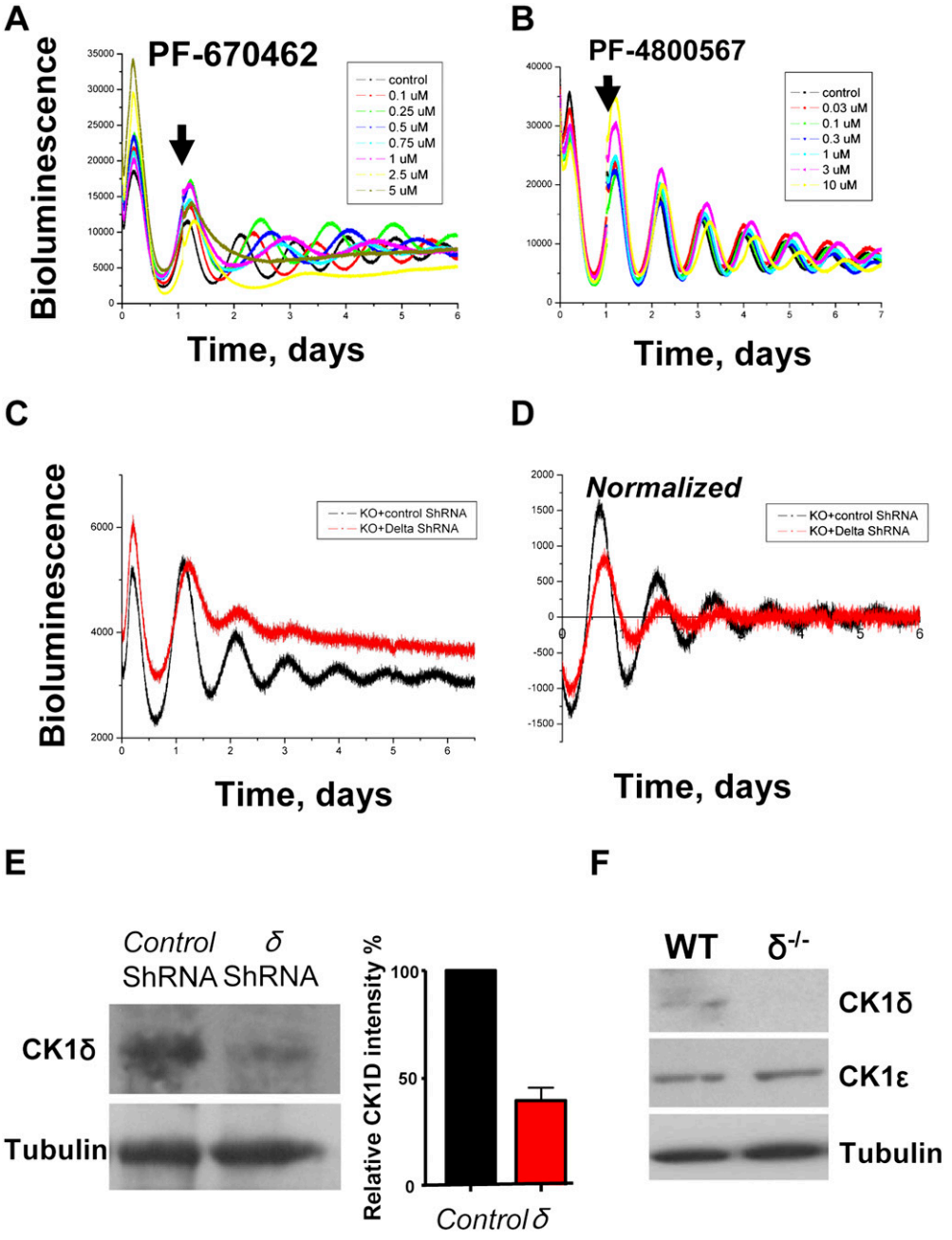

Fig. S1. Differential effects of pharmacological and genetic suppression of CK1ε and CK1δ on circadian period in WT and CK1ε mutant fibroblasts. (*A*) Representative bioluminescence recordings reveal dose-dependent prolongation of period and ultimate suppression of circadian pacemaking by PF-670462. (*B*) Representative bioluminescence recordings reveal minimal effect of PF-4800567 on circadian pacemaking with period lengthening only at highest doses. (*C* and *D*) Representative PER2::Luc bioluminescence recording from CK1ε-null fibroblasts treated with control or validated shRNA against CK1δ reveal loss of circadian gene expression in the absence of both CK1ε and CK1δ. (*C*) Raw data. (*D*) Normalized data that omitted the first 12 h of recording. Bioluminescence data were used to estimate amplitude and period of the residual oscillation and showed a net period increase (1.17 ± 0.30 h, based on the first three cycles, $P < 0.05$, $n = 3$) and reduced amplitude (δ shRNA vs. control, $n = 3$), 56.07 ± 3.69%, based on the first normalized peak. (*E*) Western blot and quantification reveal efficacy of shRNA knock down of CK1δ in *Ck1ε*$^{-/-}$ fibroblasts. (*F*) Validation of the specificity of CK1δ antibody by Western blotting. Note the absence of CK1δ in MEF cells of *Ck1δ*$^{-/-}$ mouse (gift from D. Weaver, University of Massachusetts Medical School, Worcester, MA) (1).

1. Etchegaray JP, et al. (2009) Casein kinase 1 delta regulates the pace of the mammalian circadian clock. *Mol Cell Biol* 29:3853–3866.

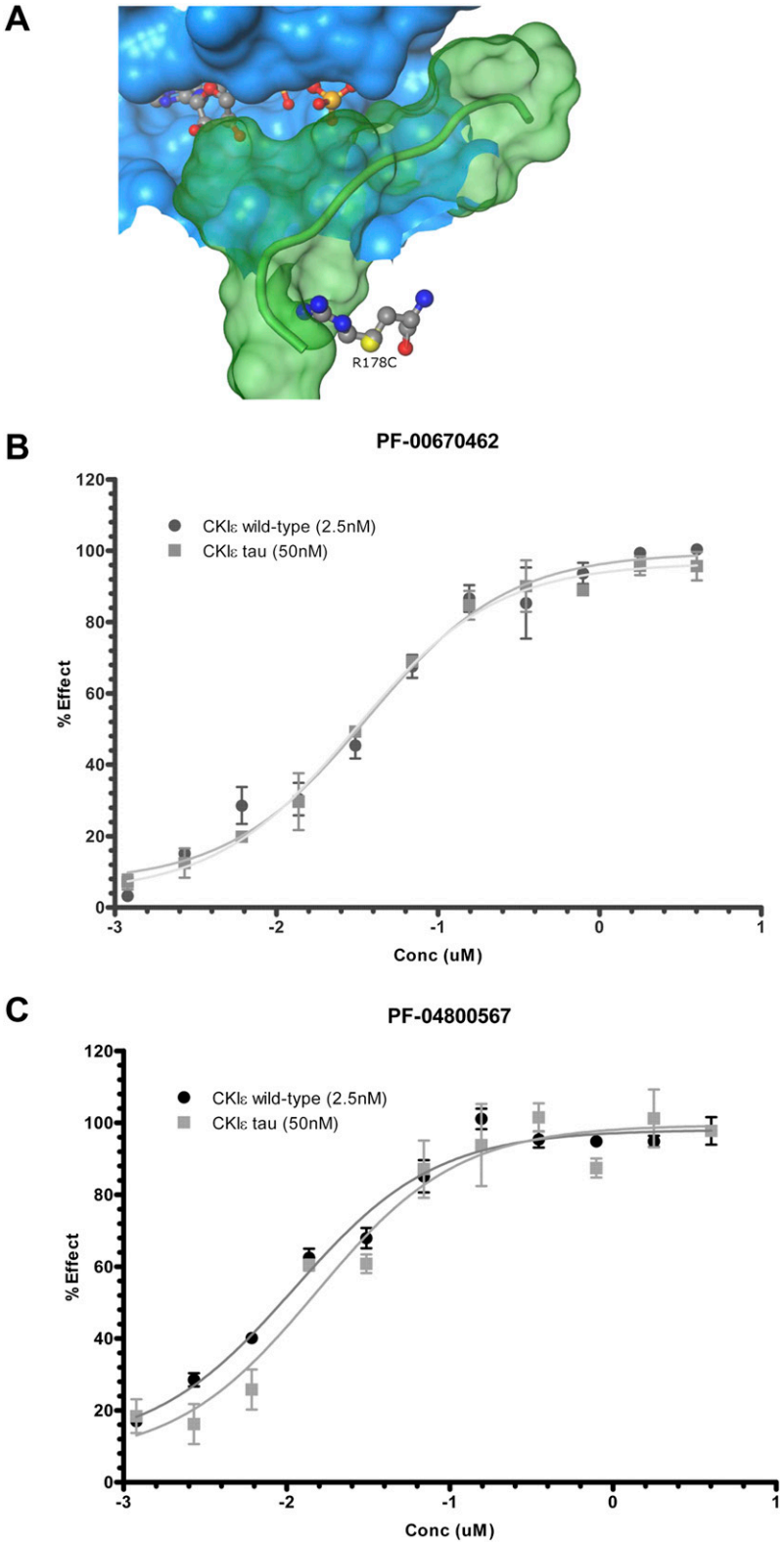

Fig. S2. Structural modeling and in vitro binding assay of CK1ε^{Tau} kinase. (*A*) Homology modeling of the human CK1ε^{tau} structure. The R178C mutation in the catalytic cleft of CK1ε^{tau} is shown as a ball and stick representation with the cysteine sulfur atom highlighted in yellow. The model strongly suggests that the R178C mutation most likely influences substrate binding and does not directly impact MgATP or ATP-competitive inhibitor binding. The peptide substrate mimetic is shown as a green ribbon and surface; the MgATP molecule is shown as a ball and stick representation and the MgATP binding pocket of CK1ε is shown as a blue surface. (*B* and *C*) In vitro binding assay suggest that both inhibitors are capable of binding to either the WT or the CK1ε^{Tau} enzyme with equivalent affinity, hence excluding the possibility that the effectiveness of PF-4800567 in CK1ε^{Tau} cells is due to altered binding.

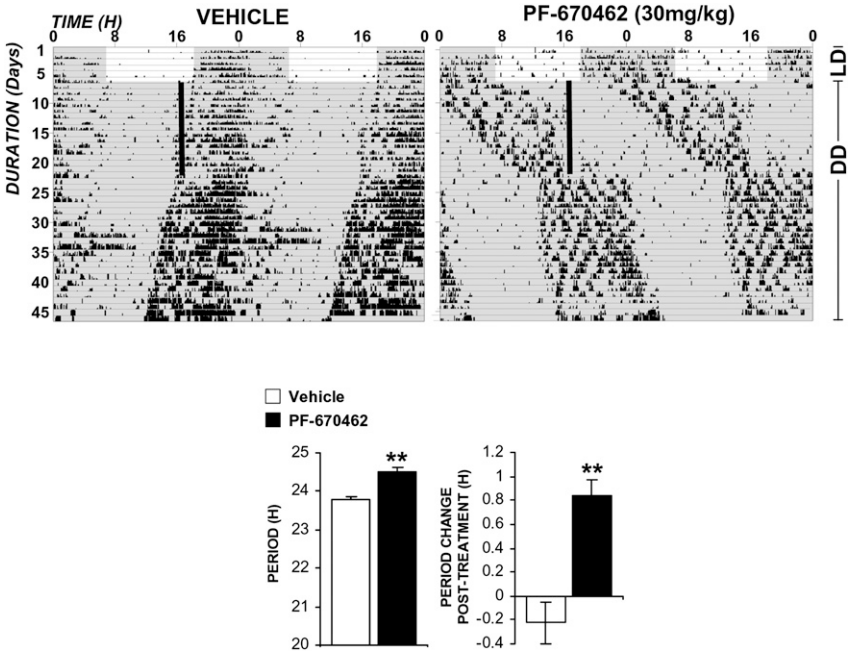

Fig. S3. Lengthening of circadian period of locomotor activity with 30 mg/kg PF-670462. Representative wheel-running actograms of WT mice treated with vehicle (*Left*) or PF-670462 (30 mg/kg/d) (*Right*) reveal no effect of daily vehicle injection but significant period lengthening by PF-670462 (n = 6 mice/group).

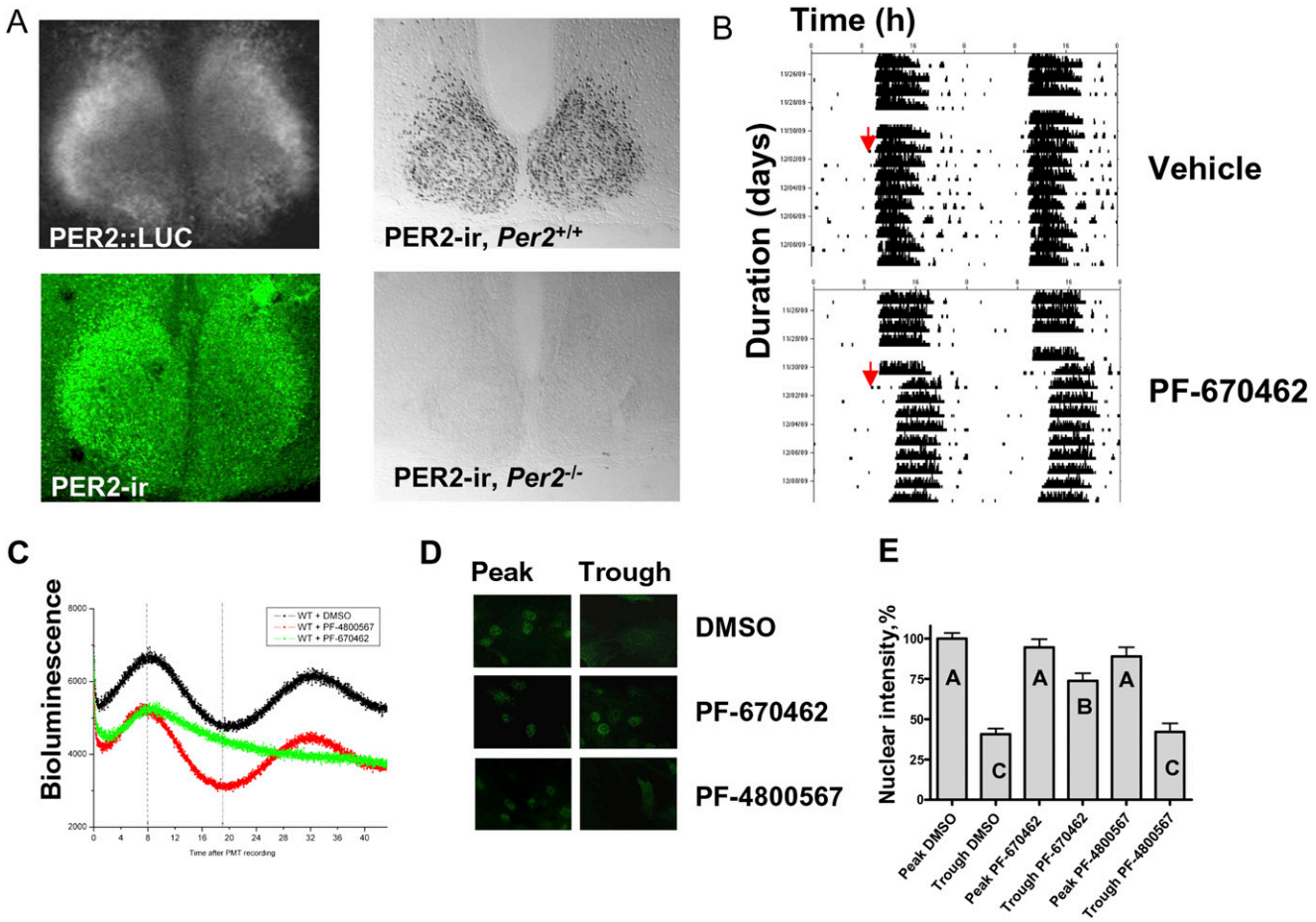

Fig. S4. Inhibition of CK1 with PF-670462 prolongs PER2 expression in SCN in vivo and fibroblasts in vitro. (*A*) Validation of PER2 antiserum by (*Left*) co-localization of PER2-ir with PER2::luciferase bioluminescence in SCN slice culture treated with PF-670462 and (*Right*) absence of PER2-ir in SCN of *Per2*$^{-/-}$ mouse. (*B*) Representative actograms demonstrate phase-delaying action of a single injection of PF-670462 (100 mg/kg) (*Lower*) but not vehicle (*Upper*). Mice were transferred from LD into DD on day of injection at ZT12 (arrow). (*C*) Representative recordings of PER2::luciferase bioluminescence reveal arrhythmia and elevation of PER2 activity in fibroblasts treated with PF-670462 (green trace) but not if treated with vehicle (black) or PF-4800567 (red). (*D*) Representative photomicrographs reveal that nuclear expression of PER2-ir is rhythmic, peaking at the height of bioluminescence emission and absent at its nadir in fibroblasts treated with vehicle or PF-4800567. Treatment with PF-670462 maintains nuclear PER2-ir. (*E*) Group data (mean ± SEM) reveal rhythmic nuclear expression of PER2-ir in presence of vehicle and PF-4800567 but significant elevation following treatment with PF-670462. Columns with same letter are not significantly different from each other.

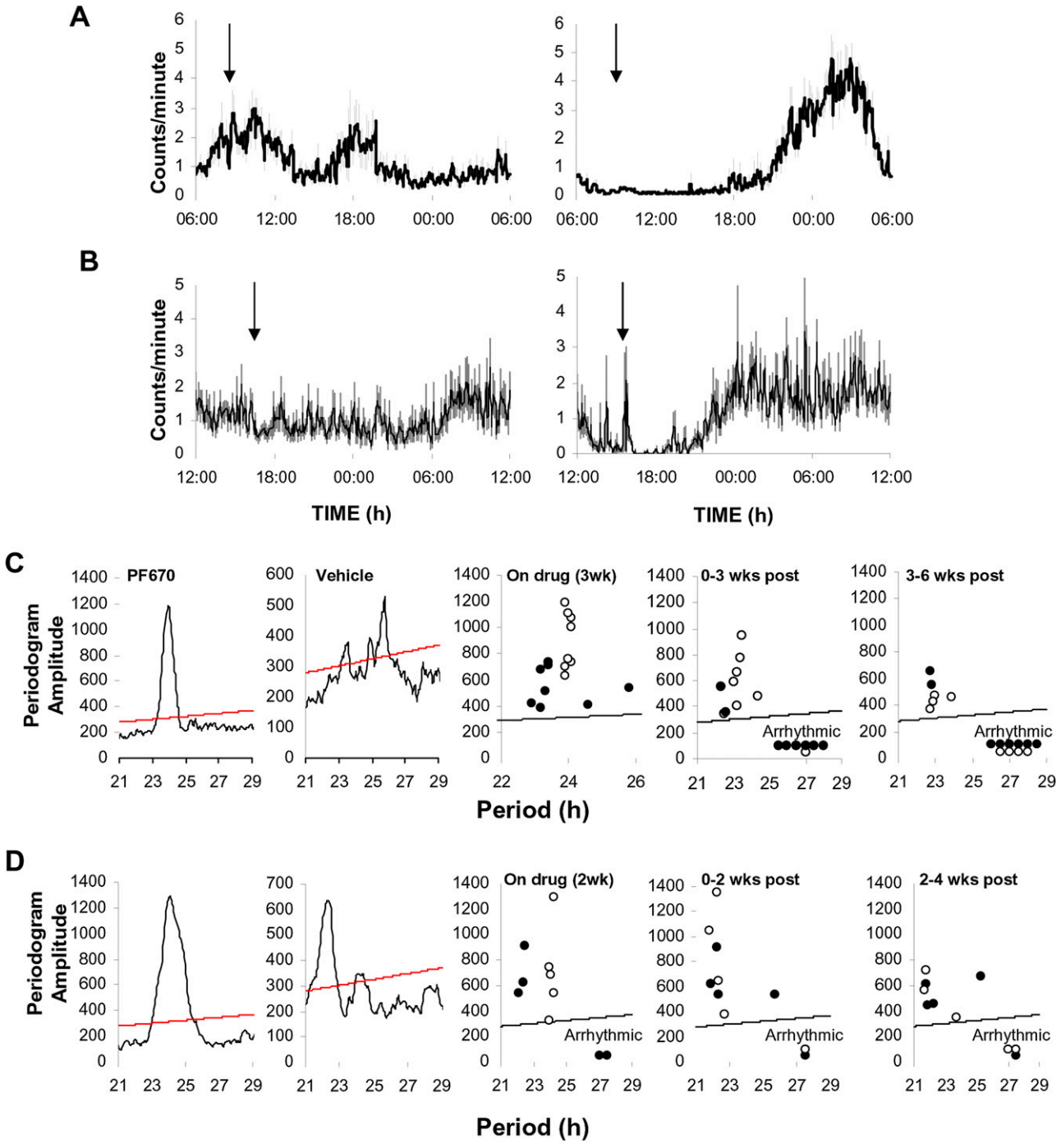

Fig. S5. Further analysis of entrainment of WT and *Vipr2*$^{-/-}$ mice by daily administration of PF-670462. (*A*) Twenty-four-hour activity profiles of WT mice housed in LL treated with vehicle (*Left*) or PF-670462 (*Right*). Profiles reflect mean daily activity across the entire dosing period. Strong entrainment is observed in the drug-treated animals, with activity onset delayed from dosing time by approximately 13 h. (*B*) Twenty-four-hour activity profiles of *Vipr2*$^{-/-}$ mice housed in DD treated with vehicle (*Left*) or PF-670462 (*Right*). Profiles reflect mean daily activity across the entire dosing period. Strong entrainment is observed in the drug-treated animals, with activity onset delayed from dosing time by approximately 6 h. (*C*) A χ^2 periodogram analysis of wheel-running activity recorded from vehicle- and PF-670462–treated WT mice housed under LL. (*Left*) Representative periodograms of vehicle- and drug-treated animals during the treatment period. (*Right*) Scatter plots display the period and amplitude of the dominant periodogram peak for each animal (○, PF-670462; ●, vehicle) during and postdrug-dosing. (*D*) A χ^2 periodogram analysis of wheel-running activity recorded from vehicle and PF-670462–treated *Vipr2*$^{-/-}$ mice housed under DD. (*Left*) Representative periodograms of vehicle- and drug-treated animals during the treatment period. (*Right*) Scatter plots display the period and amplitude of the dominant periodogram peak for each animal (○, PF-670462; ●, vehicle) during and postdrug dosing.